Accepted Manuscript

Title: Hydrogen production by methane decomposition on Pt/γ-alumina doped with neodymium catalysts and its kinetic study

Authors: M. Caballero, G. Del Angel, I. Rangel-Vázquez, L. Huerta

PII:	S0920-5861(18)30592-3
DOI:	https://doi.org/10.1016/j.cattod.2018.05.024
Reference:	CATTOD 11454
To appear in:	*Catalysis Today*
Received date:	16-12-2017
Revised date:	5-5-2018
Accepted date:	10-5-2018

Please cite this article as: Caballero M, Del Angel G, Rangel-Vázquez I, Huerta L, Hydrogen production by methane decomposition on Pt/γ-alumina doped with neodymium catalysts and its kinetic study, *Catalysis Today* (2010), https://doi.org/10.1016/j.cattod.2018.05.024

Hydrogen production by methane decomposition on Pt/γ-alumina doped with neodymium catalysts and its kinetic study

M. Caballero[1*], G. Del Angel[1*], I. Rangel-Vázquez[1], L. Huerta[2]

[1]Universidad Autónoma Metropolitana-Unidad Iztapalapa. Departamento de Química, Área de Catálisis, Av. San Rafael Atlixco No. 186, C.P. 09340, A.P 55-534. México, Ciudad de México.
[2]Instituto de Investigaciones en Materiales, Universidad Nacional Autónoma de México, Apartado Postal 70-360, 04510 México, D.F., México

[*] Corresponding author: phone number and e-mail marcabdi@yahoo.com.mx, gdam@xanum.uam.mx, 52-55-58044668.

Graphical abstract

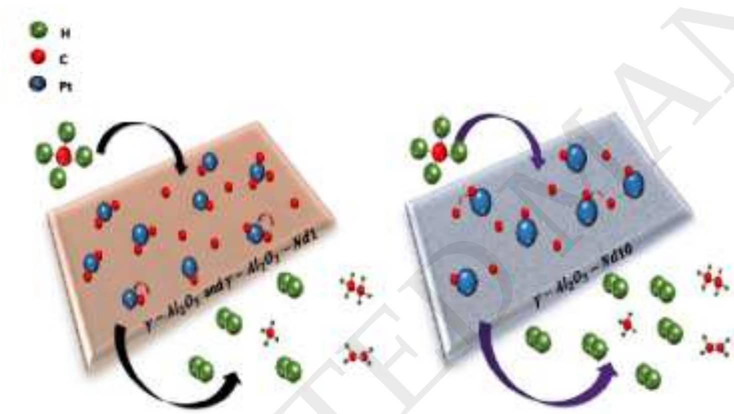

HIGHLIGHTS

- Methane decomposition on *Pt/Nd_2O_3-γ-Al_2O_3 catalysts showed 100% selectivity to H_2.*
- Interaction between Pt and γ-Al_2O_3-$Nd_2O_3$10%, favors the catalytic activity.

- The PtANd10 catalyst showed high conversion and yield.
- Weak interaction cause a spillover of the C from the platinum to the support
- Methane cracking is one kinetic order and the Ea is around 33-38 kJ/mol.

ABSTRACT:

This paper presents results for the catalytic decomposition of methane using Pt/γ-Al_2O_3 and Pt/γ-Al_2O_3-Nd_2O_3 catalysts for the hydrogen production. All catalysts were prepared by wet impregnation using $Nd(NO_3)_3 \cdot 6H_2O$ and $H_2PtCl_6.6H_2O$ as precursor salts. The concentrations of the catalysts were Pt, 1.0wt%, and Nd, 1.0 and 10.0 wt%. The reaction was carried out from 400 to 750°C.

All the catalysts reduced methane decomposition temperature by 400-750°C relative to noncatalytic thermal decomposition, which is carried out at 1300°C. the Pt catalysts supported on γ-alumina doped with neodymium exhibited higher activity than Pt supported on alumina alone. All catalysts showed high activity and selectivity at 750°C, with conversions around 57-80 %vol and hydrogen productions of 0.29, 0.27 and 0.19 mmoles of H_2/min*g_{cat} for PtANd10, PtANd1 and PtA catalyst respectively also were observed in the output stream, traces of C_2H_4 y C_2H_6 (less than 1%) and unconverted methane.

This work includes a kinetic study of methane cracking, for this purpose two experiments were carried out, the first one consisted of varying the amount of catalyst, keeping the feed flow constant, in the second experiment the flow rate was varied, keeping the mass of the catalyst constant. The activation energy of methane cracking is estimated at 35.5, 37.9 and 33 kJ/mol for the Pt/A, Pt/ANd1 and Pt/ANd10 catalysts, respectively. The characterization was done by X-ray diffraction, N_2 adsorption-desorption, H_2-TPR, FTIR of CO adsorption, FTIR of Pyridine adsorption, XPS, HRTEM, catalytic activity and TPO (Temperature programed Oxidation) analysis after reaction.

Keywords: *Rare earth, TPO determination, XPS study, particle size, acidity, activation energy.*

1. INTRODUCTION

The current need for energy is provided by the combustion of non-renewable energy sources, i.e. fossil fuels, and is associated with the release of large amounts of greenhouse gases (GHGs), especially carbon dioxide (CO_2) and other harmful gases released into the atmosphere**.**

The use of hydrogen as a fuel has been the subject of several investigations in recent years.

Extensive studies have been conducted for the development of safe, economical, and efficient hydrogen production to meet the global energy demand [1]. The main reason behind such interest is the significant decrease in greenhouse gas emission.

Another incentive to use hydrogen as a fuel is the higher efficiency achieved from its utilization in fuel cells compared to the traditional methods of electrical energy production from fossil fuels [2,3]. Although different substances can be used for producing hydrogen, the most attractive and accessible one in terms of economics, environment and technological feasibility for the near to medium term future is methane. This gas can be obtained from two major sources, namely natural gas, which is one of the most abundant fossil fuels, and biogas [4].

Hydrogen does not occur naturally in nature, but is combined with other elements such as oxygen and carbon, ie water or hydrocarbons, so these substances must be decomposed / reformed to obtain H_2 [3].

Currently, the main process for producing hydrogen is steam reforming of natural gas [5].

An attractive alternative to this method, which has recently received increased attention, is the decomposition of methane [6]. One of the advantages of this method over steam reforming is the removal of carbon dioxide from the by-products, which simplifies the process by eliminating the requirements for the separation of carbon dioxide from hydrogen and its subsequent sequestration. An overall comparison between these two processes shows that the decomposition of methane is a potential alternative to steam reforming and investigation about this process is valuable for the hydrogen economy [7]. Steam reforming is a multiple stage process.

In addition to steam reforming, partial oxidation is also used to generate hydrogen from fossil fuels [8], but the produced hydrogen is still mixed with CO and CO_2, which again needs a complicated separation process as in the steam reforming case.

Increasing demand for CO-free hydrogen has increased interest in the direct catalytic cracking of natural gas [9], described by Equation 1. The two reaction products are hydrogen and carbon, the latter being essentially in the form of filamentous carbon or carbon nanotubes [10].

$$CH_4 \rightarrow C_{(s)} + 2H_2 \qquad \Delta H° = 75.6 \text{ KJ/mol} \quad \ldots (1)$$

As a result of methane cracking, only hydrogen is produced as a gaseous product in a mixture with unreacted methane. Separation of methane and hydrogen can be achieved easily by absorption or membrane separation to produce a stream of 99% by volume hydrogen, which is much simpler than the need for further complicated separation processes that deal with CO_2 or CO [8,11].

Unlike the steam reforming process, the catalytic decomposition of methane does not include water gas shift and preferential oxidation of CO, which considerably simplifies the process and may reduce the hydrogen production costs [11]. The energy required for methane catalytic cracking is nearly one half of that required for steam reforming per mole of methane decomposed (for steam reforming $\Delta H°_{298}$ = +253.2 kJ/mol, for methane cracking $\Delta H°_{298}$ = +74.8 kJ/mol) [9,11–13]. The energy requirement is 37.4 kJ/mol H_2, in methane catalytic cracking compared to 63.3 kJ/mol H_2 in the steam reforming process [13]. In addition to the lower energy demand for methane catalytic cracking compared to steam reforming, there is no need for additional energy for steam generation or gas treatment.

The heat requirement for catalytic cracking can be covered by burning ~15-20% of the hydrogen produced, which further reduces CO_2 emissions, because CO_2 is not produced in this reaction [6].

Thermal methane cracking is not feasible at moderate temperatures. To achieve a reasonable yield, a temperature higher than 1200°C is required [14]. An active catalyst is required to obtain high methane conversion at reasonable temperatures: 500-700ºC for nickel-based catalysts, 700-950ºC for iron-based catalysts, 850-950ºC for carbon-based catalysts, and 700-1000ºC for Co, Pd, Pt, Cr, Ru, Mo, W catalysts [14,15].

Supported metal catalysts can be used to catalytically decompose hydrocarbons to produce hydrogen at more moderate temperatures. Nickel is particularly active for hydrocarbon cracking, especially for methane but present fast deactivation [16]. Cobalt and iron can also be used to catalyze methane cracking but their carbon/active site capacities are much lower than that of nickel, with additional problems in the case of cobalt, which are associated with its higher cost and toxicity [17]. Metal catalysts are usually deposited on supports such as SiO_2 or Al_2O_3 and the performance of the catalyst depends to some extent on the combination of metal and support [18].

Rare earth oxides have various fields of application, for example, in catalysis they are recognized as the most active and selective catalysts for the coupling of methane oxidation to form higher hydrocarbon products (mainly ethane and ethylene) [19]. Nd_2O_3 has high basicity and contains medium and strong basic sites, this characteristic result in a unique catalytic performance when used as active components or as supports of catalyst.

In rare earth-noble metal catalysts, rare earth materials also play an important role improving the activity, selectivity, and catalyst stability; increasing the dispersion of the active metal, and decreasing the amount of noble metal to reduce catalyst costs; also to improve poison tolerance, prolong the catalyst life and enhancing the catalyst coke-resistance [20,21].

In the literature was observed that the methane decomposition reaction showed wide ranges of activation energy (Ea) for different catalysts. Holmen et al. [22] reported an Ea value for methane decomposition, using a tubular reactor without a catalyst, of 370 kJ/mol over the temperature range of 1773−2273 K at 0.1 atm of pressure of methane. Steinberg et. al. [23] reported an Ea value of 131 kJ/mol for methane decomposition over the temperature range of 973−1173 K and around 28−56 atm of pressure, which was found to be substantially lower than the value for methane decomposition without a catalyst. Kuvshinov et al. [24] observed an Ea value of 97 kJ/mol for methane decomposition with a mixture of hydrogen over nickel catalysts. The catalyst function is to reduce the activation energy required for methane decomposition, leading to lower operating temperatures.

The purpose of the present study was to investigate the influence the addition of Nd (1 and 10 wt%) on the Pt/Al_2O_3 catalysts in the activity, selectivity and kinetic parameters for the CH_4 decomposition. The reaction was carried out at temperatures from 400 to 750°C.

The characterization by X-ray diffraction, N_2 adsorption-desorption, H_2-TPR, FTIR of CO adsorption, FTIR Pyridine of adsorption, XPS, HRTEM, Catalytic activity and TPO analysis after reaction, was performed.

2. MATERIAL AND METHODS

2.1 *Experimental Procedure. Supports and catalysts preparation*

γ-Al_2O_3 support was prepared from Boehmita Catapal B (CONDEA, high purity 99,999%, 74% AlOOH, 26% de H_2O). Firstly the Boehmite was dried to 120° C for 12 hours, then the solid was calcined in air flow of 60 mL/min for 24 h using a ramp of temperature from 25°C to 650°C. The γ-Al_2O_3-Nd_2O_3 (loaded with 1 and 10 wt% neodymium) mixed oxides, were prepared by wet impregnation of the Boehmite with the necessary quantity of $Nd(NO_3)_3 \cdot 6H_2O$ (Strem Chemicals, 99.99 %), the mixture was maintained in stirring for 3h. Then, the solids were dried in an oven to 120°C for 12 h, after that, samples were calcined at 650°C in airflow for 24 h.

The Pt catalysts were prepared by wet impregnation of the γ-Al_2O_3 and γ-Al_2O_3-Nd_2O_3 supports with the necessary quantity of $H_2PtCl_6.6H_2O$ (Aldrich 99.9 %) to obtain 1wt% of Pt. The solids were left in stirring for 3 hours, and then, the water is evaporated using a vacuum evaporator bath. Subsequently the solids were dried in an oven at 120°C, for 12 hours. The catalysts were calcined at 500°C under airflow for 5 h, finally reduced in H_2 flow at 500°C for 5 h. The Pt real percentage on the catalysts was obtained by atomic absorption technique. Catalysts were labeled as: PtANd*X*, where: Platinum, as Pt, alumina as A, neodymium as Nd, *X* is the concentration of Neodymium in wt%, AR to the catalysts after reaction and ST stability test.

2.2. Catalysts Characterization

The X-ray diffraction patterns of the supports were obtained using a D-2 phaser desktop X-ray powder diffractometer from Bruker AXS equipped with a Cu Kα radiation anode in Bragg-Brentano geometry. The detection was carried out using a LYNXEYETM detector, which is a linear-type. Intensity data was measured in continuous mode through the 2θ ranges between 10° to 70° with a 2θ step of 0.02°.

The characterization of the textural properties of the catalysts was obtained by the adsorption of N_2 at 77 K. The BET surface area of the catalysts was measured using a Quantachrome Multistation Autosorb 3B analyzer. Nitrogen was used as the measuring gas at -196°C. Before adsorption, the sample (100 mg) was outgassed at 300ºC for 24 h. The specific surface areas were calculated with the BET equation and the mean pore size by the BJH method.

The TPR determinations were carried out in a Chembet-3000 (Quantachrome Co) apparatus using 0.2 g of catalyst by means of the following protocol: samples were heated at 300°C under nitrogen flow for 30 min. Then, the samples were cooled dawn to room temperature and a mixed gas flow (5% H_2/95% N_2) was passed through the cell. The TPR profiles were recorded by heating the sample from room temperature up to 500°C at a rate of 10°C/min.

X-ray photoelectron spectroscopy analyses were performed in an ultra-high vacuum (UHV) system Scanning XPS microprobe PHI 5000 VersaProbe II. with a Al K X-ray source (hυ=

1486.6 eV), and a MCD analyzer. The surface of the samples were etched for 5 min with 1 kV Ar^+ at 0.04 μA mm^{-2}. The XPS spectra were obtained at 45º to the normal surface in the constant pass energy mode (CAE), E_0 = 100 and 10 eV for survey surface and high-resolution narrow scan, respectively. The binding energies (BE) were referenced to the Al 2p peak, the BE of which was fixed at 73.5 eV for □-Al_2O_3. In this case, the position of the C 1s line was 284.8 eV. The intensities and integration of the peaks for each of the elements were estimated by subtracting the Shirley type background and peaks adjustment performed using a mixture of Lorentzian/Gaussian curves. The XPS spectra were fitted using the SDP v 4:1 program.

Transmission electron microscopy (TEM) study was performed on an electron microscope of field emission that operates at 200 kV. The microscope is equipped with a field of Schottky type emission cannon and a configuration of ultra-high resolution (UHR) (Cs = 0.5 mm; Cc 1.1 mm; point to point resolution, 0.19 nm). The samples were also characterized by high angle annular dark field detector (HAADF) used when the microscope became operate in STEM mode known as “Z contrast”. The samples were powdered in an agate mortar and were suspended in ethanol at room temperature and dispersed in an ultrasonic bath for two minutes, then one drop of the solution was deposited on a carbon copper grid. It is important to note that the samples were transported in a plastic bag filled with argon in order to prevent the contamination of O_2. The mean Pt crystallite size for all catalysts were determined by $ds = \Sigma\, n_i d_i^3 / n_i d_i^2$ equation, where ds, is the mean crystallite size of Pt, n_i, the number of Pt crystallite diameter d_i, measured directly on the micrographs, at least 150 Pt particles were counted.

The high Resolution Transmission Electron Microscopy was determined in a HRTEM-2010F JEOL equipped with a field emission source and an acceleration of 200 kV. The sample was grinded and dispersed on a holey carbon film grid of 300 meshes, and the high-resolution images were obtained from the transmission of electrons that go through the floating sample. The measure of the crystallographic planes was done by using a Digital Micrograph program by the Gatan Software team.

FT-IR of CO adsorption spectra was determined at room temperature by using a FTIR Nicolet 170-SX apparatus, with a resolution of 2 cm^{-1}. The sample pressed in thin wafers were placed in a Pyrex glass cell, equipped with CaF_2 windows, coupled to a vacuum system and gas lines supplied. The samples were maintained under vacuum (10^{-3} Torr) at 400°C for 30 min. Then, the cell was cooled to room temperature and the CO (Praxair UHP) admission of 20 Torr was carried out. The CO excess was evacuated during 30 min, after the CO adsorbed FTIR spectra were recorded.

FT-IR of pyridine adsorption spectra was determined at room temperature by using a FTIR Nicolet 170-SX apparatus, with a resolution of 2 cm^{-1}. The catalyst is sprayed in an agate mortar and is pressed in thin wafers, which is placed in a cell, which is coupled to vacuum lines and gas lines. It is then subjected to a vacuum treatment for 30 min. ($1x10^{-3}$ Torr) at 400°C. The temperature is then lowered to 25°C and pyridine added at a pressure of 20 Torr. Subsequently, excess pyridine is evacuated under vacuum for 30 min to obtain the FTIR spectra.

The TPO study after reaction was performed to determine the amount of carbon deposited in the catalyst after reaction. The TPO determinations were carried out in a CHEMBET-3000 apparatus using a thermal conductivity detector (TCD), and 0.1 g of catalyst. In these experiments, the coke formed during the reactions was oxidized. A flow rate of 10 mL min^{-1}

of the 5% O_2/95 % He mixture was passed on the sample at a heating rate of 10◦C min^{-1}. Then, the spectra were recorded from room temperature to 750°C and keeping it at this temperature for one hour. The equipment was calibrated by sending pulses of O_2 diluted in He

2.3. Catalytic tests.

The activity determinations were carried out in a fixed bed quartz micro-reactor (i.d. = 1.2 cm and length = 56 cm) at atmospheric pressure and catalyst load of 0.05 g. The reaction temperatures varied from 400 to 700°C, the increase of temperature was on steps of 100ºC and the last at 750ºC with a rate of 5ºC min^{-1}. Experiments consisted in a previous thermal treatment to the catalysts with flowing nitrogen for 15 min at room temperature. Then, a pure CH_4 (99.999 %) feed steam (2 mL min^{-1}) was introduced into the reactor. The inlet and outlet effluents were monitored on line gas chromatograph, Shimadzu GC-2014 equipped with 6 packed columns and TCD and FID detectors. Which allows the measurement of inorganic gases (H_2, CO and CO_2) and organic hydrocarbons as CH_4, C_2H_4, and C_2H_6. The identification of reaction products were accomplished by the quantification of them, which were carried out with calibration curves of products reaction using the appropriate software. The methane conversion was calculated as the amount of methane converted throughout the experiment over the amount admitted during that step. The selectivity was the amount of each product H_2, C_2H_4, or C_2H_6 collected at reactor outlet over the methane converted. The yield was calculated with (% Conversion * % Selectivity H_2).

2.4. kinetic Study.

A kinetic study of the decomposition reaction of methane in the temperature range of 400 - 750°C under atmospheric pressure was also carried out. A fixed bed quartz reactor was used to investigate the kinetics and to evaluate the parameters of the model, for this purpose two experiments were carried out, the first consisted of varying the amount of catalyst, keeping the feed flow constant, in the second experiment the flow rate was varied, keeping the mass of the catalyst constant.

3. Results and Discussion

3.1 Catalysts Characterization

The XRD patterns of the Pt catalysts after reduction at 500°C for 5 h are showed in Fig. 1. The catalysts show the characteristic peaks of γ-alumina phase (JCPDS PDF 056-0457 Quality: Rietveld). The lines associated with PtO (PDF 42-0866) were not observed in this sample, neither signals corresponding to Pt crystals (JCPDS 04-0802) were detected in any of the catalysts studied. This is explained by a low Pt concentration and small Pt particles, which could not be detected by the equipment.

Also no peaks for $Nd(OH)_3$ (PDF 06-0601) nor Nd_2O_3 (1 and 10 wt%) (JCPDS PDF 01-079-9858 Quality: Star (*)) were detected. The diffraction pattern of PtANd1 catalyst does not show notable difference in respect to that observed in PtA catalyst. However, in PtANd10 catalyst a modification of the diffraction pattern is observed. The alumina peaks in that catalyst shows lower intensity that in the PtA and PtANd1 catalysts, which indicate low crystallinity of the PtANd10 catalyst. The presence of neodymium at 10 wt. % inhibited the growth of the alumina crystals [25]. In Fig. 1 is plotted an inset where is observed the peaks of the alumina having a maxima at around 67° in 2θ. The increase in the broad is related with the reduction of the crystallite size as the concentration of Nd_2O_3 increases.

The type of isotherms of adsorption-desorption presented by the catalysts are shown in Figure 1, are classified according to the IUPAC as type IV [26], which is characteristic of mesoporous materials. On the other hand, the hysteresis type for the catalysts is type H1 [27].

The BET specific surface areas of the supports and fresh catalysts are reported in Table 1. The increased surface area in the ANd1 support relative to □-alumina can be attributed to the neodymium which completely blocks the pores of □-alumina and for ANd10 support neodymium is not fully dispersed and partially blocks the pores of the □-alumina (see table 1). The incorporation of platinum (1wt. % nominal) to the aforementioned materials, the area decreases in all cases respect to the supports. However, the pore volume decreases by about 5% for catalysts with neodymium; this indicates that platinum contributes to the reduction in size of the pore in a consistent manner for both materials (see inset figure 1). The pore volume and pore diameter of PtA catalyst (Table 1) remained constant with respect to bare γ-alumina support (0.54 nm and 12.3 nm respectively). That means that platinum is over the γ-alumina surface, therefore there are no changes in the distribution and volume of pore.

The concentrations of Pt on the catalysts were determined by atomic absorption and reported in Table 1. The nominal concentration of Pt was 1.0wt%, the real concentrations are 0.51, 0.60 and 0.83 wt%, and these values can be considered valid, in the error range.

The TPR profile of PtA, PtANd1 and PtANd10 catalysts are showed in Fig.2. At least three temperature peak profiles were detected. The first one (from low to higher temperatures), corresponding to the reduction of PtO_2 species [28]. The second one arises from the reduction of oxy- or hydroxychlorinated Pt species [28], and the third one, it has been assigned to the bulk phase of the PtOx and to highly dispersed particles with different degree of interaction on the support, as previously reported [29,30].

The PtA and PtANd1 present similar broad temperature profile of 156 and 157°C for the first signal while 302 and 300°C respectively for the second. Whereas for the third, the temperatures signal specie are 434 and 432°C respectively, in both cases the temperature is analogous although the peak in PtA is slightly more intense than in PtANd1 catalyst. In this last, the hydrogen consumption is smaller. The effect of the addition of 1wt% of Nd is notable mainly in the low amount of hydrogen for the reduction of the PtOx specie, which represent a higher size of particle and can be conclude that in these two catalysts, the interaction Pt-Al_2O_3-N_2O_3 is high. On PtANd10 catalyst, the temperature for the first reduction specie is 155°C in agreement to the PtA and PtANd1 catalysts. However the temperature of reduction for the second and third specie are shifted at lower temperatures 268 and 428°C than the aforementioned catalysts, indicating that in PtANd10 catalyst the interaction of Pt in surface is weak and mainly with neodymium oxide, Pt-Nd_2O_3, which concentration is in great proportion on the surface, favoring the reduction of the Pt species.

The XPS technique was used to determine the binding energies (Table 2) of the chemical species of the elements and the proportions on the surface of the fresh catalysts, after reaction (PtANd10AR) and stability test (PtANd10ST). To determine the stability test of the PtANd10 catalyst, the sample, was maintained in time on stream for 10 h at 750°C.

Literature [31,32] reports an overlap of the Al 2p core level of the support with the most intense lines of the active phase of platinum Pt 4f core level. Therefore, the study of platinum in this region is complicated for the allocation of the currents and the binding energies.

Therefore, another platinum signal (Pt 4d core level) is chosen for the study. This lower-intensity line no longer overlap with another spectral line of another compound.

In Figure 3, the high-resolution XPS spectra of platinum corresponding to the core level spectra of Pt $4d_{5/2}$ in the range of 305.00-340.00 eV are shown. In the deconvolution of the platinum spectra, it was observed two components in the fresh samples, (Table 2). The first component with a binding energy of 313.40 eV is correlated to reduced platinum Pt°, according to that reported by several authors [31,33,34]. The following binding energy at 315.60 eV is associated with the PtO specie [33,35]. An explanation of the presence of the PtO species is given by the authors [33] that by reducing the catalyst at 500°C, they observe that the platinum maintains a $\square^{+}$ character, which indicates that there is a strong interaction between the metal and the support. It has been reported that by impregnating platinum and calcined it in different supports such as Al_2O_3, CeO_2 and La_2O_3 [31] the proportions of the reduced and oxidized platinum species were affected. This causes the platinum has a positive character with respect to the support (electron deficiency) and was correlated by the charge transfer of the platinum to the support.

Although the catalysts of PtA and PtANdX were reduced to 500°C for 5 hours in hydrogen flow, platinum particles in the oxidized state prevailed (Table 2). However, by incorporating different proportions of neodymium (1 and 10 wt%) the ratio of species Pt°/$Pt^{\delta+}$ decreases and the PtO species is found in greater proportion in PtANd1 with respect to the PtA reference, this effect was correlated by the charge transfer of the metal to the support as mentioned above.

In figure 3, the high resolution spectra of core level Nd $4p_{3/2}$ are shown where two spectral lines were observed, whose binding energies are placed in 229.00 and 224.50 eV corresponding to Nd_2O_3 and Nd $(OH)_3$ respectively. The addition of 1% of neodymium to the PtANd1 catalyst present a Pt° specie diminution, favoring the oxidized $Pt^{\delta+}$ specie (44%). Higher concentration of neodymium (10%) in the PtANd10 catalyst, the Pt° species increases at 72.7%. The Nd_2O_3 and $Nd(OH)_3$ are species present in both PtANd1 and PtANd10 catalysts with Nd_2O_3 percentages of 84.1% and 90.6% respectively and the rest corresponds to $Nd(OH)_3$ specie. The high abundance of Nd_2O_3 on the surface of the catalyst, with the highest concentration of this compound (PtANd10) favors the presence of Pt° species.

The increase of the platinum oxidized species on the PtANd1 catalyst after the treatment in H_2 flow at 500 ° C can be attributed to the transfer of charge of platinum to neodymium, keeping platinum in a deficient state of electrons [36]. This change observed can be attributed to a weakening of the bonding force Nd-O in the presence of Pt, which leads to a high mobility of reticular oxygen in PtANd1. While in the catalyst PtANd10 with greater amount of Nd_2O_3, this specie present greater stability, decreasing the transfer of change between Pt and Nd [36]. That explain the return of the original value of Pt° specie in the PtANd10 catalyst

The oxygen spectrum (O 1s) shows for the PtA catalyst a binding energy of 530.74 eV, however, when adding neodymium at different proportions this energy is shifted to lower energies (530.53 – 530.47 eV) this could be due to that neodymium and produces in the alumina structural and textural changes favoring a greater interaction between both compounds [37].

The histograms of the distribution of particle size determined by TEM (Fig. 4), for PtA and PtANdX fresh catalysts. The PtA catalyst was observed platinum highly dispersed, with mean particle diameter around 1.6 nm, the dispersion corresponding to this value was 71%. The catalysts with neodymium (1 and 10 wt%) had an important fraction of particles with mean diameter greater than 2 nm, with dispersions of 54 and 48% respectively, the mean Pt particle sizes measured by FTIR-CO, were confirmed with the values obtained by TEM, Z contrast (Table 1).

The HRTEM image of the PtANd10 catalyst is shown in Figure 5, which was examined by several zones with boxes a), b), c), and d). Later these zones were worked using the FFT-HRTEM for each of the boxes. In the right part of Figure 5 the FFT of the examined areas showed several interplanar distances, these were assigned to different crystalline phases in the following way. The distance 1.31 and 2.28 Å correspond to the crystallographic planes (442) and (222) belonging to -alumina with card number JCPDS 00-056-0457 Quality: Rietveld. The distance 1.96 Å corresponds to the plane (200) of metallic platinum with card number JCPDS 04-0802. The distances 1.06 and 1.91 Å correspond to the planes (213) and (110) correspond to the numbered Nd_2O_3 of card JCPDS 01-079-9858 Quality: Star (*). Finally the distances 1.30 and 1.84 Å were found, these correspond to the planes (302) and (300) of the crystalline $Nd(OH)_3$ phase with PDF card number 06-0601 and the distances 1.34 and 2.17 Å corresponding to the planes (202) and (110) of the crystalline PtO phase with PDF card number 42-0866.

The adsorption of CO as a test molecule is a technique by which Pt catalysts supported on γ-alumina can be characterized by FTIR. The deconvolution of FTIR-CO spectra for platinum monometallic catalysts (1 wt% Pt) supported on γ-Al_2O_3 and γ-Al_2O_3 modified with 1 and 10 wt% neodymium are shown in Figure 6. For the FTIR-CO spectrum of PtA, PtANd1 and PtANd10 different bands were detected between 1930-1700 cm^{-1}. This region was assigned to the multiple bond of the CO molecule adsorbed on platinum [38], other authors consider the weak band in 1850 cm^{-1} corresponds to the bridged link Pt^0-CO-Pt^0 [39] and the 1784 cm^{-1} band corresponds to CO adsorbed is triply bounded to Pt [40].

The region located between 2010-1990 cm^{-1}, is correlated with the linearly bound CO species in metallic platinum in an isolated corner (Pt^0-CO isolated corners). The next region in the range of 2080-2040 cm^{-1}, is attributed to the linear carbonyl bond of CO with metallic platinum [41]. Other authors correlate it with adsorption of linear CO in the platinum metal particle in a corner (Pt^0-CO corners) in the range of 2066-2041 cm^{-1} and the region latter localed between 2162-2158 cm^{-1} is correlated to the oxidized platinum species (Pt^{2+}-CO) which occurs at 2134 cm^{-1} [42].

The Figure 6 shows slight displacement in the CO absorbed species in the Pt metallic, which can be due to the presence of neodymium. In addition, it was observed that with the increase in the neodymium load, there was an increase in the IR intensity of the linear CO adsorption band that could be related to the Pt crystallite size increase (Table 1) said catalysts present suitable sites for a greater adsorption of methane.

The results obtained by FT-IR spectroscopy-pyridine adsorption, allowed elucidating the amount of Brönsted acid and Lewis acid sites present in the samples. It has been proposed that the metal–support interaction is associated with the acidity/alkalinity of the support [43,44]. With increasing support alkalinity, electron transfer between the support oxygen atoms and the nearby metal particles can increase the electron density on the metal particles. The peaks at 1448 and 1614 cm^{-1} showed the existence of Lewis acid sites, while no adsorption band characteristic of Brönsted acid sites at 1540 cm^{-1} was observed. Considering the high basicity of the neodymium respect to the alumina, it can be inferred that the decrease of the acidic sites in the materials with neodymium can be due to the high dispersion of this on the surface of the γ-Al_2O_3 blocking the acid sites (Table 1). In the case of Al_2O_3 doped with Nd_2O_3 (Figure not showed) the intensity bands associated with Lewis acidity were much lower, this result indicated that Nd_2O_3 decreased the number of Lewis acid sites. The fact that the acidity decreases could indicate that the additive (neodymium), selects very acid sites in the support to be deposited as it has mentioned in its study Oudet et. al. [45].

The samples after reaction were characterized by Fourier-pyridine transform spectroscopy; the results show that the Lewis-type acidity is maintained. However, the total acidity of the fresh PtA catalyst (258 μmol/g_{cat}) decreases considerably after the reaction (92 μmol/g_{cat}) and for the fresh PtANd10 material its value is 213 μmol/g_{cat} and after reaction gives 74 μmol/g_{cat}. In both cases the acidity decreases to one third of the original value, this may be due to the fact that coke forms is anchored in the active sites of the metal.

3.2. Activity, Selectivity and coke deposited.

Methane dehydrogenation was conducted at temperatures of 400, 500, 600, 700 and 750ºC with undiluted methane flow and a space velocity of 6 L $h^{-1}g^{-1}$. Figure 7 shows the profiles of methane conversion as function of temperature. It can be seen that the conversion of methane increases as the temperature increases from 400ºC to a maximum conversion at 750ºC. The PtA catalyst present a conversion of 64 % at 750°C and activity per site (TOF) of 34.2 h^{-1} with the crystallite size of 1.6 nm, this catalyst shows a production of hydrogen of 0.19 $mmol_{H2}/min*g_{cat}$. While the PtANd1 catalyst exhibits a behavior similar to the PtA catalyst, with a conversions of 56.8% a 750°C, and TOF of 33.6 h^{-1} with the crystallite size of 2.1 nm, this catalyst shows the highest molar flow of 0.27 $mmol_{H2}/min*g_{cat}$. The PtANd10 catalyst, presents the highest production at 750°C, with a conversion of 80% of methane (Table 3), crystallite size of 2.4 nm, TOF of 38.6 h^{-1} and one molar flow of 0.29 mmol $_{H2}/min*g_{cat}$ (Figure 8).

The presence of a large proportion of oxidized species of Pt affected the catalytic activity of the PtA and PtANd1 catalysts due to a strong interaction between the metal and the support. On the contrary, in the PtANd10 catalyst an increase on the catalytic activity was observed due to the presence of neodymium, which favors a lower metal support interaction, leading to a rapid desorption of the reaction products. As it was observed in the characterization by H_2-TPR and XPS of these catalysts.

On the other hand, the determination of the particle size for the PtANd10_AR catalyst, by TEM using the contrast Z method, showed that the particles size increased notably from 2.4 nm (fresh catalyst), to 10.5 nm (after reaction) a sintering of the catalyst was observed by a temperature effect. The particle size raise, then the structure and morphology of the Pt particles changed at high temperature (750°C). This is explained by lower interaction of the Pt nanoparticles on Al_2O_3-Nd_2O_3 support, which favors the sintering of Pt particles leading to formation of large Pt particles at 750°C.

Comparing the conversion at 500°C (50.5 vol%) and at 750°C (80.0 vol%) is observed that large Pt particles plays an important role in CH_4 conversion. The values of activity and selectivity (see Table 3) increase with the increase of particle size, then the reaction of methane dehydrogenation was sensitive to particle size [46].

In previous studies, it was analyzed that chlorine is retained in the alumina support surface in Pt catalysts with low metal loading after reduction under hydrogen flow at 400 °C, and that the amount of residue remaining in the catalyst after reduction depends largely on the choice of support material. There is a good consensus that platinum does not coordinate directly with chlorine in the post-reduction state.

Chloride ions from the precursor at a short distance from the active metal particles hinder the adsorptive and catalytic properties of the metal. For this reason, catalyst precursor has an important effect in catalyst activity, e.g. in the hydrogenation and oxidation of hydrocarbons [47]. In our case, the catalysts were calcined in air at 500°C under airflow for 5 h and finally reduced in H2 flow at 500°C for 5 h, after the treatment the amount of residual chlorine was found around 0.3% at. By analysis of EDS and XPS, said percentage remained constant before and after the reaction. In our case, we detected that the chlorine residual improve the activity for the cracking of methane reaction.

The carbon contents of the used Pt catalysts obtained by TPO analysis are showed in Figure. 9, noble metal catalysts are more tolerant toward coking than conventional nickel catalysts. Higher activity together with the better resistance toward coking extends catalyst lifetime, making the use of noble metals feasible [48].

Temperature-programmed oxidation (TPO) has been widely used to determine the amount of carbon deposited on the catalyst after reaction [49,50]. In the present case it was investigated the differences in the reactivity of coke formed on Pt catalysts by through oxidation of the coke on the catalyst surface followed by TPO. The temperature at which oxidation occurs is determined by the location and chemical nature of the coke species. Since metals catalyze oxidation, the location is represented by the distance from the active metal. Moreover, the more graphitic forms of coke oxidize at high temperatures [51]. Different forms of coke can thus be classified with respect to their chemical nature and location on the catalyst [41,50].

The area under a TPO profile (Figure 9) represents, the total amount of CO_2 formed in the course of one TPO experiment. The total amount of CO_2 was used to calculate the relative amount of coke deposited on the catalysts during the reaction (Table 4).

In the TPO profiles, a shift to lower oxidation temperatures is observed, as the neodymium content was increased. In the TPO profiles for the coke formed in the reaction until 750°C, coke oxidation begins around 80°C, coke that oxidized at temperatures < 200 °C is assumed to be located on the active metal since metals catalyze oxidation. The CO_2 maxima peaks located between 500-600°C, suggests that, the coke was located on the metal or metal-support interface, and that the nature of the carbonaceous species was uniform, therefore, the deposits are polyaromatic and their composition depends very much on the reactant. Their formation involves hydrogen transfer (acid catalysts) and dehydrogenation; and coke that oxidized at high temperatures (>700°C) is considered to be more graphitic and located on the support rather than on the active metal [41,52]. The coke formation was greater on the PtA catalyst with 4.77%, followed by PtANd10 catalyst with 3.51%, and the catalyst with less coke formation was PtANd1 catalyst with 2.84%, due to the low conversion of methane in this catalyst. The PtANd1 catalyst showed lower amount of coke deposited, since the conversion of methane was also lower at all temperatures of reaction with respect to the PtA and PtNd10 catalysts. Methane cracking and hydrogen yield increased significantly with increasing reaction temperature from 400 to 750 ° C. The maximum hydrogen yield of 79.9%, 63.9% and 56.7% was achieved on the catalysts PtANd10, PtA and PtANd1 respectively, at 750 ° C, showing the same tendency at all reaction temperatures.

During the temperature-programmed oxidation, CO_2 was detected, and the temperature for CO_2 evolution over the PtANd10 catalyst is much lower than those over the PtANd1 and PtA catalysts. This suggested that the carbon species deposited on the PtANd10 catalyst is more active than those on the PtANd1 and PtA catalysts and that were more near the metal [52].

Table 2 e Total amount of coke after ATR of n-hexadecane

3.3. Kinetics of the reaction, pseudo-order of reaction and activation energies

The rate of decomposition of methane was strongly dependent on the temperature, the methane flow and the mass of the catalyst. By increasing the flow rate in the fixed bed, the contact efficiency between methane and catalyst particles decreased, and therefore methane conversion decreased [53,54].

Assuming a plug flow for the gaseous phase flowing through the catalyst bed, integration of the differential mass balance conducted on the catalyst yielded the following equation:

$$\frac{W_{cat}}{F_{CH40}} = \int_0^{X_{CH4}} \frac{dx_{CH4}}{r_{CH4}} \quad \ldots (2)$$

Substitution of $r_{CH4} = K_n * C_{CH4}^n$ y $F_{CH40} = v_0 * C_{CH40}$ in equation (2)

$$\frac{W_{cat}}{v_0 * C_{CH40}} = \int_0^{X_{CH4}} \frac{dX_{CH4}}{K_n * C_{CH4}^n} \quad \ldots (3)$$

In addition, for gas phase expansion reaction the relationship between C_{CH4} and initial methane concentration C_{CH40} is defined as:

$$C_{CH4} = C_{CH40} \frac{1 - X_{CH4}}{1 + \varepsilon X_{CH4}} \quad \ldots. (4)$$

The result of the equation is as follows:

$$\frac{W_{cat}}{v_0} = \frac{C_{CH40}^{1-n}}{K_n} \int_0^{X_{CH_4}} \left\{ \frac{[1 + \varepsilon X_{CH_4}]}{[1 - X_{CH_4}]} \right\}^n dX_{CH_4} \quad \ldots (5)$$

where v_0 is the methane flow in L/min, n is the order of the methane decomposition reaction and K_n is the kinetic constant ($L(g_{cat}\ min)^{-1}(mol\ L^{-1})^{1-n}$ and ε is the expansion factor equal to 1 according to the equation (1).

Equation (5) was used to determine the pseudo-order n and the kinetic constant K_n by plotting of $\frac{W_{cat}}{v_0}$ versus the value of the integral shown in the right-hand side of equation (5). These were carried out to the experimental data reported in Table 5 for experiments with variation of catalyst mass (Fig. 10) and for experiments with variation in methane feed flow (Fig. 11), separately. For that purpose, various values of n were tried (n = 0, 0.5, 1, 1.5 and 2) and best fits were obtained with n = 1 (correlation coefficient > 0.99 and >0.97) for experiments with variation of catalyst mass (Fig. 10) and (correlation coefficient > 0.99 and >0.98) for experiments with variation in methane feed flow (Fig. 11). The value of k_n was calculated from the slope 4.1 - 4.75 (L/g_{cat} min).

In order to find k_n at temperatures of 400, 500, 600, 700 and 750°C, the value of the integral of equation (5) was found according to the data of each experiment and then the value of k_n was calculated.

The activation energy was calculated by using an Arrhenius plot of ln k against 1/T (Fig. 12) and the slope of the linear plot is (-Ea/R). The activation energy, the value of the pre-exponential factor and the Arrhenius equation reads in the Table 6:

4. *Conclusions*

A larger metal particle size, lower acidity and a surface rich on neodymium oxide of PtANd10 catalyst favored a high catalytic activity.

A surface rich on neodymium oxide leads to a weak surface interaction between Pt and Nd_2O_3-γ-Al_2O_3 support, improving the catalytic activity due to an easy desorption of the products. That weak interaction can also cause a spillover of the carbon obtained after reaction from the platinum to the support.

It is interesting to note that the selectivity to hydrogen in all the catalysts was 100%.

The apparent kinetics shows that the reaction order is 1 and activation energy is 33 kJ/mol for PtANd10 catalyst, 37.9 kJ/mol for PtANd1 catalyst and 35.5 kJ/mol for PtA catalyst; concluding that the best catalyst was PtANd10.

Acknowledgements

We acknowledge to CONACYT for the support provided to the project SEP-CONACYT CB-2013-01-220191 and Marina Caballero Diaz thanks to the CONACYT for the grant awarded No 387137/255851.

REFERENCES

[1] S.K. Saraswat, B. Sinha, K.K. Pant, R.B. Gupta, Kinetic Study and Modeling of Homogeneous Thermocatalytic Decomposition of Methane over a Ni–Cu–Zn/Al_2O_3 Catalyst for the Production of Hydrogen and Bamboo-Shaped Carbon Nanotubes, Ind. Eng. Chem. Res. 55 (2016) 11672–11680. doi:10.1021/acs.iecr.6b03145.

[2] S. Farhad, F. Hamdullahpur, Developing fuel map to predict the effect of fuel composition on the maximum voltage of solid oxide fuel cells, J. Power Sources. 191 (2009) 407–416. doi:10.1016/j.jpowsour.2009.02.073.

[3] S. Farhad, F. Hamdullahpur, Developing fuel map to predict the effect of fuel composition on the maximum efficiency of solid oxide fuel cells, J. Power Sources. 193 (2009) 632–638. doi:10.1016/j.jpowsour.2009.03.054.

[4] S. Farhad, M. Younessi-Sinaki, M.R. Golriz, F. Hamdullahpur, Exergy analysis and performance evaluation of CNG to LNG converting process, Int. J. Exergy. 5 (2008) 164–176. doi:10.1504/IJEX.2008.016673.

[5] A. Malaika, B. Krzyzyńska, M. Kozłowski, Catalytic decomposition of methane in the presence of in situ obtained ethylene as a method of hydrogen production, Int. J. Hydrogen Energy. 35 (2010) 7470–7475. doi:10.1016/j.ijhydene.2010.05.026.

[6] N. Muradov, Hydrogen via methane decomposition: An application for decarbonization of fossil fuels, Int. J. Hydrogen Energy. 26 (2001) 1165–1175. doi:10.1016/S0360-3199(01)00073-8.

[7] M. Steinberg, Fossil fuel decarbonization technology for mitigating global warming, Int. J. Hydrogen Energy. 24 (1999) 771–777. doi:10.1016/S0360-3199(98)00128-1.

[8] N. Muradov, Thermocatalytic Co2 - Free Production of Hydrogen From

Hydrocarbon Fuels, Proc. 2002 U.S. DOE Hydrog. Progr. Rev. NREL/CP-610-32405. (2002) 1–19. doi:NREL/CP-570-28890.

[9] M. a. Ermakova, D.Y. Ermakov, Ni/SiO2 and Fe/SiO2 catalysts for production of hydrogen and filamentous carbon via methane decomposition, Catal. Today. 77 (2002) 225–235. doi:10.1016/S0920-5861(02)00248-1.

[10] N. Catón, J.I. Villacampa, C. Royo, E. Romeo, A. Monzón, Hydrogen production by catalytic cracking of methane using Ni-Al2O3 catalysts. Influence of the operating conditions, Stud. Surf. Sci. Catal. 139 (2001) 391–398. doi:10.1016/S0167-2991(01)80222-6.

[11] N.Z. Muradov, How to produce hydrogen form fossil fuels without \ce{CO2} emission, Int. J. Hydrogen Energy. 18 (1993) 211–215.

[12] S. Takenaka, H. Ogihara, I. Yamanaka, K. Otsuka, Characterization of silica-supported Ni catalysts effective for methane decomposition by Ni K-edge XAFS, J. Synchrotron Radiat. 8 (2001) 587–589. doi:10.1107/S0909049500015879.

[13] A.M. Dunker, S. Kumar, P.A. Mulawa, Production of hydrogen by thermal decomposition of methane in a fluidized-bed reactor - Effects of catalyst, temperature, and residence time, Int. J. Hydrogen Energy. 31 (2006) 473–484. doi:10.1016/j.ijhydene.2005.04.023.

[14] H.F. Abbas, W.M.A. Wan Daud, Hydrogen production by methane decomposition: A review, Int. J. Hydrogen Energy. 35 (2010) 1160–1190. doi:10.1016/j.ijhydene.2009.11.036.

[15] S. Takenaka, H. Ogihara, I. Yamanaka, K. Otsuka, Decomposition of methane over supported-Ni catalysts: Effects of the supports on the catalytic lifetime, Appl. Catal. A Gen. 217 (2001) 101–110. doi:10.1016/S0926-860X(01)00593-2.

[16] L.B. Avdeeva, D.I. Kochubey, S.K. Shaikhutdinov, Cobalt catalysts of methane decomposition : accumulation of the ® lamentous carbon, 177 (1999). doi:10.1016/S0926-860X(98)00250-6.

[17] M.A. Ermakova, D.Y. Ermakov, G.G. Kuvshinov, Effective catalysts for direct cracking of methane to produce hydrogen and filamentous carbon. Part I. Nickel catalysts, Appl. Catal. A Gen. 201 (2000) 61–70. doi:10.1016/S0926-860X(00)00433-6.

[18] Y. Echegoyen, I. Suelves, M.J. Lázaro, R. Moliner, J.M. Palacios, Hydrogen production by thermocatalytic decomposition of methane over Ni-Al and Ni-Cu-Al catalysts: Effect of calcination temperature, J. Power Sources. 169 (2007) 150–157. doi:10.1016/j.jpowsour.2007.01.058.

[19] G.A.M. Hussein, Rare earth metal oxides: Formation, characterization and catalytic activity thermoanalytical and applied pyrolysis review, J. Anal. Appl. Pyrolysis. 37 (1996) 111–149. doi:10.1016/0165-2370(96)00941-2.

[20] R. Burch, Knowledge and know-how in emission control for mobile applications, Catal. Rev. - Sci. Eng. 46 (2004) 271–333. doi:10.1081/CR-200036718.

[21] M. Shelef, R.W. McCabe, Twenty-five years after introduction of automotive catalysts: what next?, Catal. Today. 62 (2000) 35–50. doi:10.1016/S0920-5861(00)00407-7.

[22] A. Holmen, O.A. Rokstad, A. Solbakken, High-Temperature Pyrolysis of Hydrocarbons. 1. Methane to Acetylene, Ind. Eng. Chem. Process Des. Dev. 15 (1976) 439–444. doi:10.1021/i260059a017.

[23] M. STEINBERG, Production of hydrogen and methanol from natural gas with reduced CO2 emission, Int. J. Hydrogen Energy. 23 (1998) 419–425.

doi:10.1016/S0360-3199(97)00092-X.

[24] G.G. Kuvshinov, Y.I. Mogilnykh, D.G. Kuvshinov, Kinetics of Carbon Formation from CH4-H2 Mixtures over a Nickel Containing Catalyst, Catal. Today. 42 (1998) 357–360. doi:10.1016/S0920-5861(98)00115-1.

[25] I. Rangel-Vázquez, G. Del Angel, V. Bertin, F. González, A. Vázquez-Zavala, A. Arrieta, J.M. Padilla, A. Barrera, E. Ramos-Ramirez, Synthesis and characterization of Sn doped TiO<inf>2</inf> photocatalysts: Effect of Sn concentration on the textural properties and on the photocatalytic degradation of 2,4-dichlorophenoxyacetic acid, J. Alloys Compd. 643 (2015) S144–S149. doi:10.1016/j.jallcom.2014.12.065.

[26] S. Lowell, J.E. Shields, M.A. Thomas, M. Thommes, Adsorption Isotherms, in: 2004: pp. 11–14. doi:10.1007/978-1-4020-2303-3_3.

[27] K.S.W. Sing, Reporting physisorption data for gas/solid systems with special reference to the determination of surface area and porosity (Recommendations 1984), Pure Appl. Chem. 57 (1985) 603–619. doi:10.1351/pac198557040603.

[28] A. Borgna, T.F. Garetto, C.R. Apesteguía, F. Le Normand, B. Moraweck, Sintering of Chlorinated Pt/γ-Al2O3 Catalysts: An In Situ Study by X-Ray Absorption Spectroscopy, J. Catal. 186 (1999) 433–441. doi:10.1006/jcat.1999.2557.

[29] C. Meephoka, C. Chaisuk, P. Samparnpiboon, P. Praserthdam, Effect of phase composition between nano γ- and χ-Al2O3on Pt/Al2O3catalyst in CO oxidation, Catal. Commun. 9 (2008) 546–550. doi:10.1016/j.catcom.2007.04.016.

[30] A.C.S.F. Santos, S. Damyanova, G.N.R. Teixeira, L. V. Mattos, F.B. Noronha, F.B. Passos, J.M.C. Bueno, The effect of ceria content on the performance of Pt/CeO 2/Al2O3 catalysts in the partial oxidation of methane, Appl. Catal. A Gen. 290

(2005) 123–132. doi:10.1016/j.apcata.2005.05.015.

[31] G. Del Angel, A. Bonilla, Y. Peña, J. Navarrete, J.L.G. Fierro, D.R. Acosta, Effect of lanthanum on the catalytic properties of PtSn/γ-Al2O3bimetallic catalysts prepared by successive impregnation and controlled surface reaction, J. Catal. 219 (2003) 63–73. doi:10.1016/S0021-9517(03)00140-4.

[32] G. Del Angel, A. Bonilla, J. Navarrete, E.G. Figueroa, J.L.G. Fierro, The inhibiting effect of lanthanum on the formation of benzene over PtSn/Al2O3reforming catalysts, J. Catal. 203 (2001) 257–263. doi:10.1006/jcat.2001.3330.

[33] J.C. Serrano-Ruiz, G.W. Huber, M.A. Sánchez-Castillo, J.A. Dumesic, F. Rodríguez-Reinoso, A. Sepúlveda-Escribano, Effect of Sn addition to Pt/CeO2-Al2O3and Pt/Al2O3catalysts: An XPS,119Sn Mössbauer and microcalorimetry study, J. Catal. 241 (2006) 378–388. doi:10.1016/j.jcat.2006.05.005.

[34] M. García-Diéguez, I.S. Pieta, M.C. Herrera, M.A. Larrubia, I. Malpartida, L.J. Alemany, Transient study of the dry reforming of methane over Pt supported on different γ-Al2O3, Catal. Today. 149 (2010) 380–387. doi:10.1016/j.cattod.2009.07.099.

[35] M.J. Tiernan, O.E. Finlayson, Effects of ceria on the combustion activity and surface properties of Pt/Al2O3catalysts, Appl. Catal. B Environ. 19 (1998) 23–35. doi:10.1016/S0926-3373(98)00055-1.

[36] I. Tankov, K. Arishtirova, J.M.C. Bueno, S. Damyanova, Surface and structural features of Pt/PrO2-Al2O 3 catalysts for dry methane reforming, Appl. Catal. A Gen. 474 (2014) 135–148. doi:10.1016/j.apcata.2013.08.030.

[37] J. Jayasree, Acid-base properties of binary oxide catalysts of alumina rare earth oxides, Indian J. Chem. Sect. a-Inorganic Bio-Inorganic Phys. Theor. Anal. Chem.

38 (1999) 56–60.

[38] L.-C. de Me´norval, A. Chaqroune, B. Coq, A. François Figueras, Characterization of mono- and bi-metallic platinum catalysts using CO FTIR spectroscopy Size effects and topological segregation, J. Chem. Soc. Faraday Trans. 93 (1997) 3715–3720. doi:10.1039/a702174g.

[39] O. Dulaurent, D. Bianchi, Adsorption isobars for CO on a Pt/Al2O3 catalyst at high temperatures using FTIR spectroscopy: isosteric heat of adsorption and adsorption model, Appl. Catal. A Gen. 196 (2000) 271–280. doi:10.1016/S0926-860X(99)00472-X.

[40] N. Hérault, L. Olivet, L. Pirault-Roy, C. Especel, M.A. Vicerich, C.L. Pieck, F. Epron, Controlled preparation and characterization of Pt-Rh/Al2O3bimetallic catalysts for reactions in reducing conditions, Appl. Catal. A Gen. 517 (2016) 81–90. doi:10.1016/j.apcata.2016.02.024.

[41] A. Shamsi, J.P. Baltrus, J.J. Spivey, Characterization of coke deposited on Pt/alumina catalyst during reforming of liquid hydrocarbons, Appl. Catal. A Gen. 293 (2005) 145–152. doi:10.1016/j.apcata.2005.07.002.

[42] V.J. Cybulskis, J. Wang, J.H. Pazmiño, F.H. Ribeiro, W.N. Delgass, Isotopic transient studies of sodium promotion of Pt/Al2O3for the water-gas shift reaction, J. Catal. 339 (2016) 163–172. doi:10.1016/j.jcat.2016.04.018.

[43] Neopentane Conversion Catalyzed by Pd in L Zeolite.pdf, (n.d.).

[44] G. Larsen, G.L. Haller, Metal-support effects in Pt/L-zeolite catalysts, Catal. Letters. 3 (1989) 103–110. doi:10.1007/BF00765061.

[45] E.S.P.B. V, F. Oudet, A. Vejux, P. Courtine, Evolution During Thermal Treatment of Pure and Lanthanum-Doped Pt / Al , O , and Pt-Rh / Al , O , Automotive Exhaust

Catalysts Transmission Electron Microscopy Studies on Model Samples, 50 (1989) 79–86.

[46] S. Theme, Catalytic decomposition of methane over supported Ni, (2009) 814–820. doi:10.1002/apj.

[47] N.W. Cant, D.E. Angove, M.J. Patterson, The effects of residual chlorine on the behaviour of platinum group metals for oxidation of different hydrocarbons, 44 (1998) 93–99.

[48] R.K. Kaila, A.O.I. Krause, Autothermal reforming of simulated gasoline and diesel fuels, Int. J. Hydrogen Energy. 31 (2006) 1934–1941. doi:10.1016/j.ijhydene.2006.04.004.

[49] M. Guisnet, P. Magnoux, Organic chemistry of coke formation, Appl. Catal. A Gen. 212 (2001) 83–96. doi:10.1016/S0926-860X(00)00845-0.

[50] S. Srihiranpullop, P. Praserthdam, A new approach of coke characterization on metal and support for Pt/Al 2O3 by combination of Al2O3 and Pt/SiO2, Catal. Today. 93–95 (2004) 723–727. doi:10.1016/j.cattod.2004.06.067.

[51] N. Martı, M. Viniegra, E. Lima, G. Espinosa, Coke Characterization on Pt / Al2O3 - beta-Zeolite Reforming Catalysts, Ind. Eng. Chem. Res. 43 (2004) 1206–1210. doi:10.1021/ie034007b.

[52] M, 13 Part A: Chapter 7: Deactivation and Regeneration, in: Handb. Heterog. Catal., 1997: pp. 1263–1282. doi:10.1002/9783527619474.ch7.

[53] J.L. Pinilla, I. Suelves, M.J. Lázaro, R. Moliner, Kinetic study of the thermal decomposition of methane using carbonaceous catalysts, Chem. Eng. J. 138 (2008) 301–306. doi:10.1016/j.cej.2007.05.056.

[54] M.J. Lázaro, J.L. Pinilla, I. Suelves, R. Moliner, Study of the deactivation

mechanism of carbon blacks used in methane decomposition, Int. J. Hydrogen Energy. 33 (2008) 4104–4111. doi:10.1016/j.ijhydene.2008.05.072.

Figure Captions

Figure 1. XRD patterns of the PtA, PtANd1 and PtANd10 fresh catalysts.

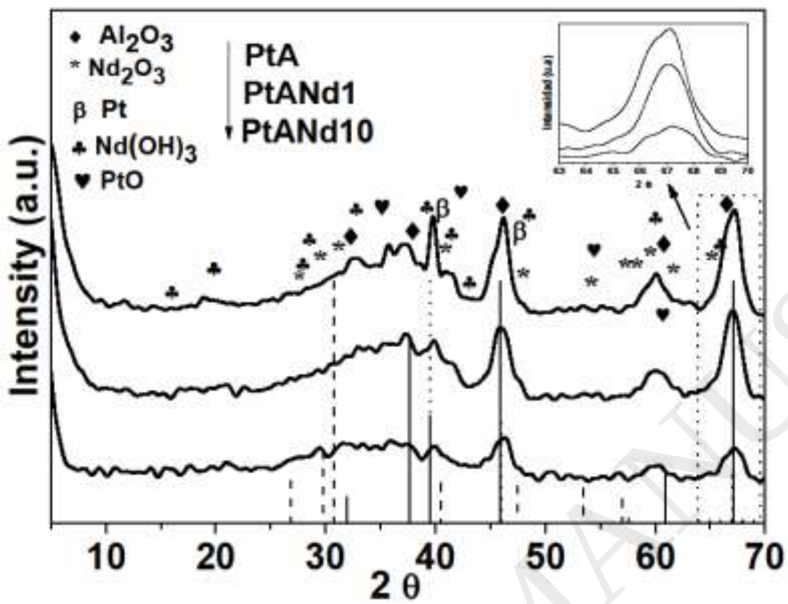

Figure 2. H_2-TPR profiles of neodymium promoted PtA and PtANd1 and PtANd10 catalysts.

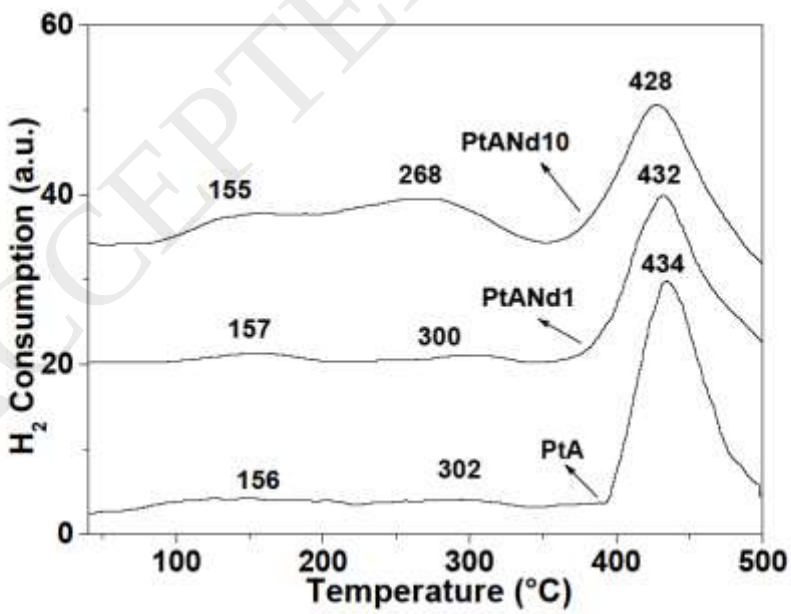

Figure 3. XPS spectra in the platinum region (Pt 4d) of the PtA and (Nd 4p) PtANdX fresh catalysts and the PtANd10 catalysts after reaction (AR) and stability test (ST).

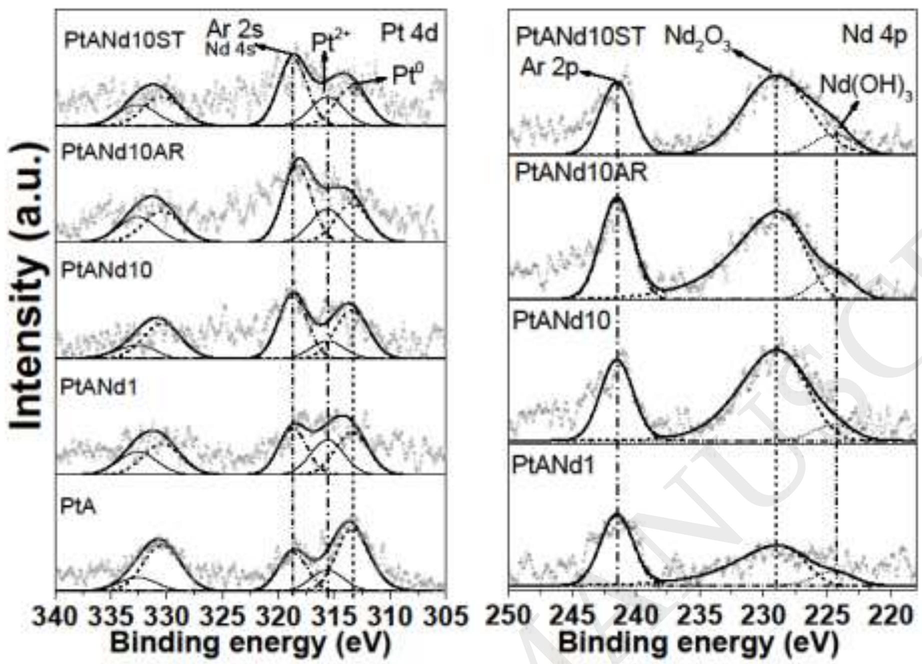

Figure 4. TEM images and histograms of metal crystallite size distribution for the PtA, PtANd1 and PtANd10 fresh catalysts.

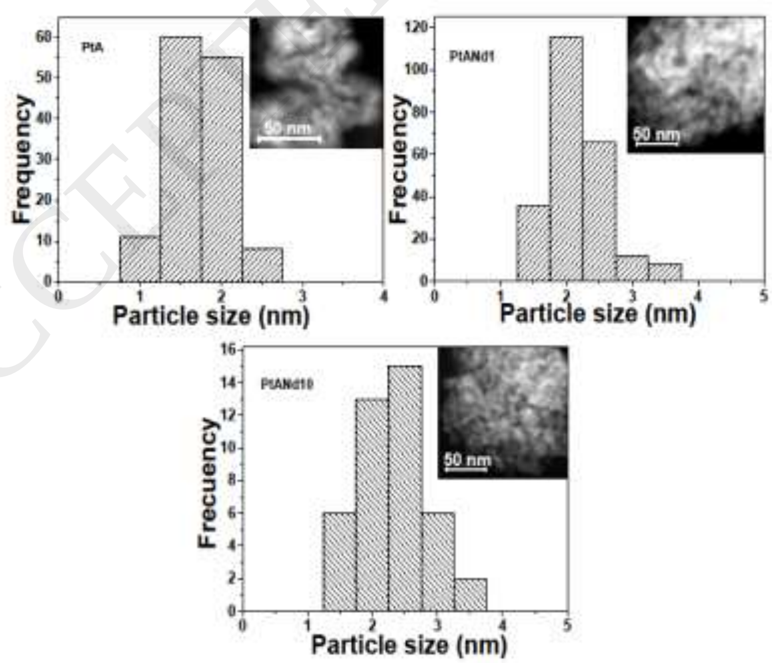

Figure 5. HRTEM images of PtANd10 catalyst with a), b), c) and d) corresponding to FFT of the scanned areas.

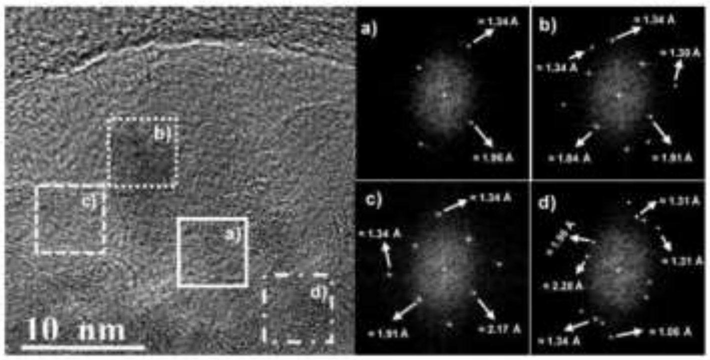

Figure 6. Deconvolution of CO infrared spectra of Pt catalysts supported on γ-Al $_2O_3$ and γ-Al_2O_3 modified with neodymium 1 and 10 wt%, a) PtA, b) PtANd1 y c) PtANd10.

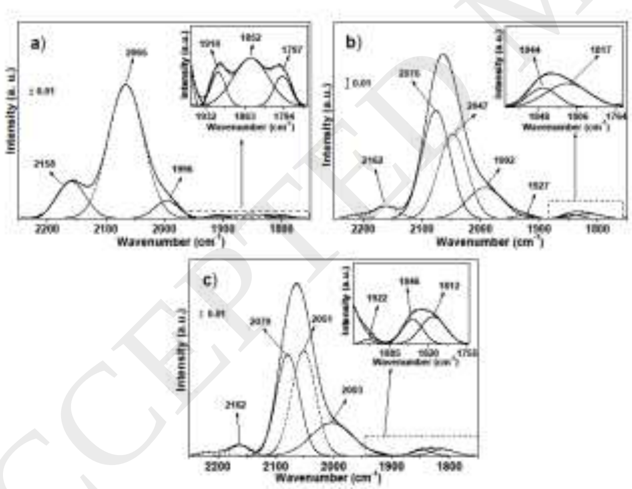

Figure 7. Profiles of methane conversion as function of temperature

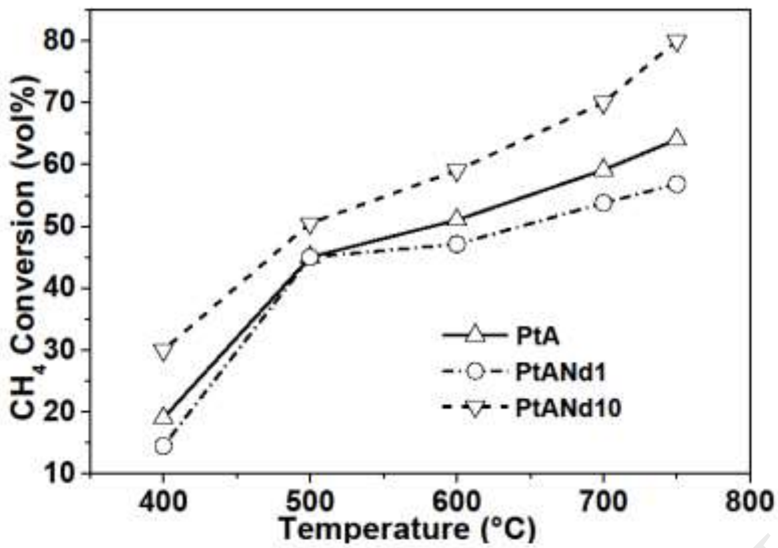

Figure 8. H_2 Production (milimol$_{H2}$/min*g$_{cat}$) as function of temperature.

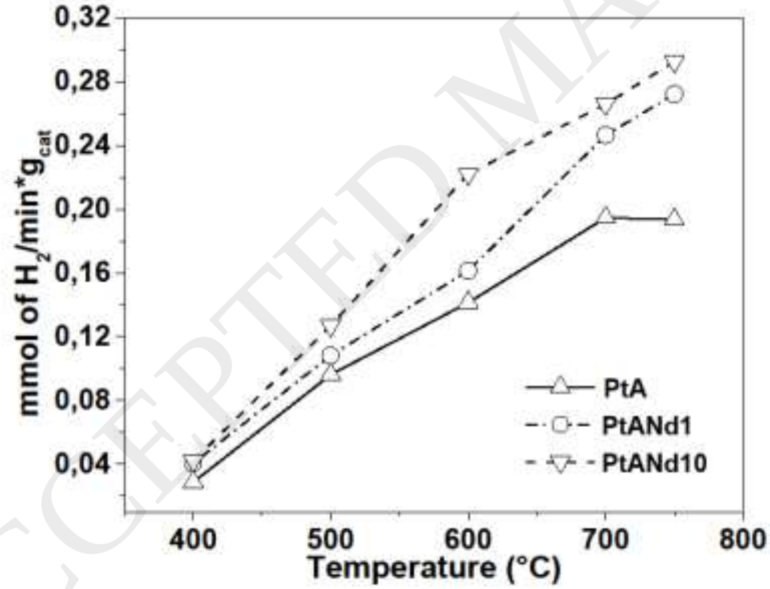

Figure 9. TPO profiles of PtA (a), PtANd1 (b) and PtANd10 (c) catalysts after reaction.

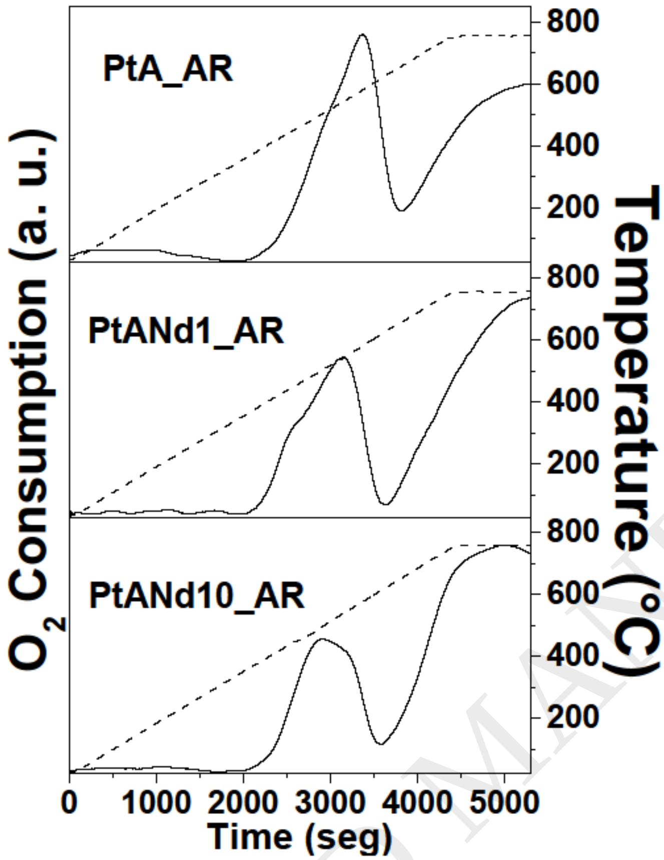

Figure 10. Pseudo order of reaction to T and υo constants and variable catalyst mass for PtA, PtANd1 and PtANd10 fresh catalysts.

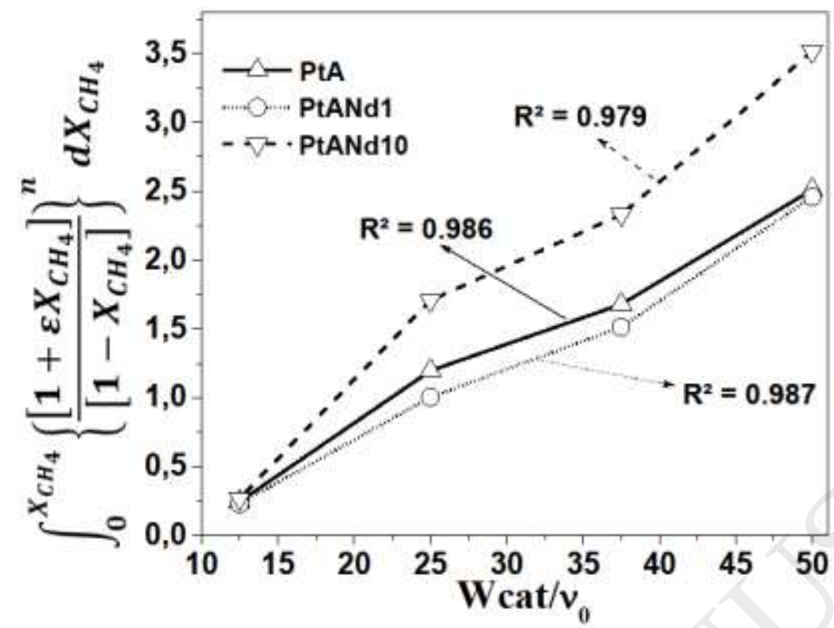

Figure 11. Pseudo order of reaction to T and W_{cat} constants and $\upsilon_o$variable for PtA, PtANd1 and PtANd10 fresh catalysts.

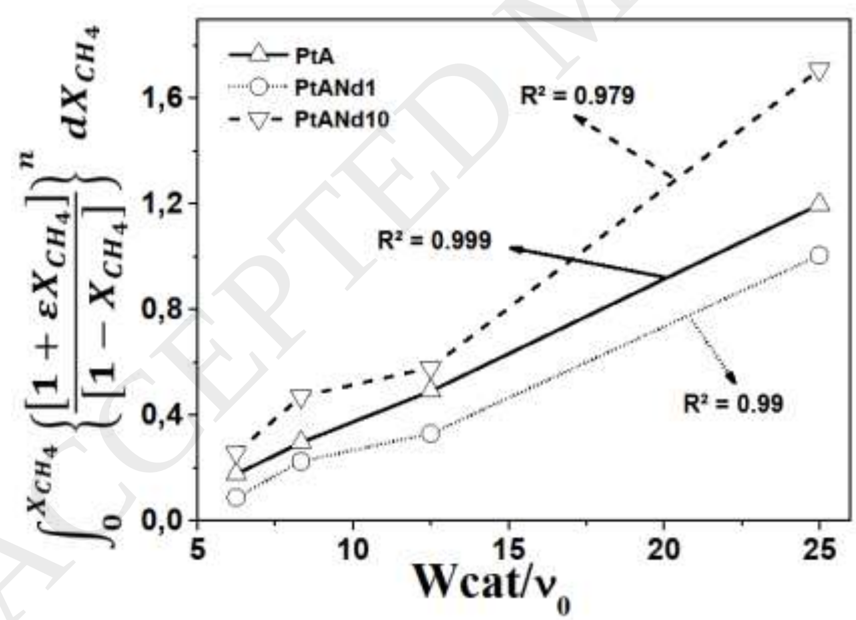

Figure 12. Arrhenius plot of ln k vs. (1/T).

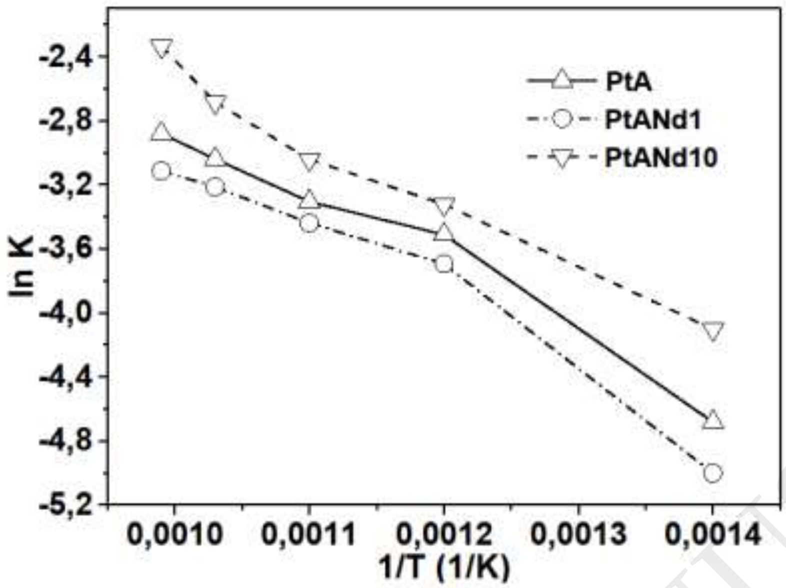

PtA
PtANd1
PtANd10
ln K
-2,4
-2,8
-3,2
-3,6
-4,0
-4,4
-4,8
-5,2
0,0010
0,0011
0,0012
0,0013
0,0014
1/T (1/K)

Table

Catalyst	BET Area (m^2/g)	Pore Volume (cc/g)	Pore Diameter (nm)	Acidity Total[a] (μmol/g_{cat})	d[b] (nm)	d[c] (nm)	Pt[d] (wt%)	% D[e]
PtA A*	147 (163)	0.54 (0.54)	12.3 (12.3)	258	1.6±0.32	1.95	0.51	71
PtANd1 ANd1*	150 (188)	0.48 (0.51)	9.6 (9.6)	239	2.1±0.48	2.55	0.60	54
PtANd10 ANd10*	146 (169)	0.35 (0.37)	7.4 (7.8)	213	2.4±0.57	2.7	0.83	48

Table 1. Characteristics of the Pt catalysts

[a] Total lewis acidity reported at 150 °C
[b] d = mean metal crystallite size by TEM
[c] d = mean Pt particle size measured by FTIR-CO
[d] Atomic Absorption Technique
[e] Dispersion (%) = ([a]$N_{(S)}$ Pt/[b]$N_{(T)}$ Pt) x 100.[a]$N_{(S)}$ Pt=Number of active Platinum atoms available for reaction. [b]$N_{(T)}$ Pt=Total number of Platinum atoms in the catalyst material.
* Corresponds to the fresh support without platinum and between parenthesis ( ) is the values obtained from the characterization of the supports by means of nitrogen adsorption

Table 2. Binding energies (eV) found by XPS for Platinum (Pt 4d), Oxygen (O 1s) and Neodymium (Nd 4p) for the different fresh and used catalysts (after reaction and stability test in the production of hydrogen)

	Platinum	PtO	Oxygen	Neodymium	
Sample	(Pt^0)	(Pt^{2+})		Nd_2O_3	$Nd(OH)_3$
	Pt $4d_{5/2}$	Pt $4d_{5/2}$	O 1s	Nd $4p_{3/2}$	Nd$4p_{3/2}$
	(eV)				
PtA	313.40 (75.9)*	315.60 (24.1)	530.74 (100)	-	-
PtANd1	313.40 (56.0)	315.60 (44.0)	530.53 (100)	229.00 (84.1)	224.50 (15.9)
PtANd10	313.40 (72.7)	315.60 (27.3)	530.51 (100)	229.00 (90.6)	224.50 (9.4)
PtANd10AR	313.40 (54.6)	315.60 (45.4)	530.53 (100)	229.00 (85.7)	224.50 (14.3)
PtANd10ST	313.40 (57.4)	315.60 (42.6)	530.47 (100)	229.00 (86.4)	224.50 (13.6)

*Percentage of abundance of each of the species.

Table 3. Conversion, TOF, selectivity and yield for the methane dehydrogenation on PtA and PtANd*X* at 750ºC.

Catalyst	Conversion (%)	TOF (h^{-1})	Selectivity H_2 (%)	Yield (%)
PtA	64	34.2	99.9	63.9
PtANd1	57	33.6	99.9	56.7
PtANd10	80	38.6	99.9	79.9

Table 4. Total amount of coke in the PtA and PtANd1 and PtANd10 catalysts after reaction.

Catalysts	Coke ($mass_{coke}/mass_{cat}$, %)
PtA	4.77
PtANd1	2.84
PtANd10	3.51

Table 5. Experimental data used to determine the pseudo-order

	Experiments with variation of catalyst mass		Experiments with variation in methane feed flow	
Temperature (°C)	Catalyst Mass (mg)	Methane Feed Flow (mL/min)	Catalyst Mass (mg)	Methane Feed Flow (mL/min)
750	25	2	50	2
750	50	2	50	4
750	75	2	50	6
750	100	2	50	8

Table 6. Activation energy, value of the pre-exponential factor and Arrhenius equation

Catalyst	Activation energy (KJ/mol)	Value of the pre-exponential factor (L/g_{cat} min)	Arrhenius equation
Pt/A	35.5	4.1	$k = 4.131745678e^{\left(\frac{-4285}{T}\right)}$
Pt/ANd1	37.9	4.6	$k = 4.614022333e^{\left(\frac{-4564.2}{T}\right)}$
Pt/ANd10	33	4.75	$k = 4.753114085e^{\left(\frac{-4070}{T}\right)}$